Eribulin mesilate suppresses experimental metastasis of breast cancer cells by reversing phenotype from epithelial–mesenchymal transition (EMT) to mesenchymal–epithelial transition (MET) states

T Yoshida[1], Y Ozawa[1], T Kimura[2], Y Sato[2], G Kuznetsov[3], S Xu[3], M Uesugi[2], S Agoulnik[3], N Taylor[3], Y Funahashi[3] and J Matsui*,[1]

[1]Discovery Biology, Oncology Product Creation Unit, Eisai Co., Ltd, Tsukuba, Ibaraki 300-2635, Japan; [2]Biomarkers and Personalized Medicine, Core Function Unit, Eisai Co., Ltd, Tsukuba, Ibaraki 300-2635, Japan and [3]Biomarkers and Personalized Medicine, Core Function Unit, Eisai Inc., Andover, MA 01810, USA

Background: Eribulin mesilate (eribulin), a non-taxane microtubule dynamics inhibitor, has shown trends towards greater overall survival (OS) compared with progression-free survival in late-stage metastatic breast cancer patients in the clinic. This finding suggests that eribulin may have additional, previously unrecognised antitumour mechanisms beyond its established antimitotic activity. To investigate this possibility, eribulin's effects on the balance between epithelial–mesenchymal transition (EMT) and mesenchymal–epithelial transition (MET) in human breast cancer cells were investigated.

Methods: Triple negative breast cancer (TNBC) cells, which are oestrogen receptor (ER −)/progesterone receptor (PR −)/human epithelial growth receptor 2 (HER2 −) and have a mesenchymal phenotype, were treated with eribulin for 7 days, followed by measurement of EMT-related gene and protein expression changes in the surviving cells by quantitative real-time PCR (qPCR) and immunoblot, respectively. In addition, proliferation, migration, and invasion assays were also conducted in eribulin-treated cells. To investigate the effects of eribulin on TGF-β/Smad signalling, the phosphorylation status of Smad proteins was analysed. In vivo, the EMT/MET status of TNBC xenografts in mice treated with eribulin was examined by qPCR, immunoblot, and immunohistochemical analysis. Finally, an experimental lung metastasis model was utilised to gauge the metastatic activity of eribulin-treated TNBC in the in vivo setting.

Results: Treatment of TNBC cells with eribulin in vitro led to morphological changes consistent with transition from a mesenchymal to an epithelial phenotype. Expression analyses of EMT markers showed that eribulin treatment led to decreased expression of several mesenchymal marker genes, together with increased expression of several epithelial markers. In the TGF-β induced EMT model, eribulin treatment reversed EMT, coincident with inhibition of Smad2 and Smad3 phosphorylation. Consistent with these changes, TNBC cells treated with eribulin for 7 days showed decreased capacity for in vitro migration and invasiveness. In in vivo xenograft models, eribulin treatment reversed EMT and induced MET as assessed by qPCR, immunoblot, and immunohistochemical analyses of epithelial and mesenchymal marker proteins. Finally, surviving TNBC cells pretreated in vitro with eribulin for 7 days led to decreased numbers of lung metastasis when assessed in an in vivo experimental metastasis model.

Conclusions: Eribulin exerted significant effects on EMT/MET-related pathway components in human breast cancer cells in vitro and in vivo, consistent with a phenotypic switch from mesenchymal to epithelial states, and corresponding to observed decreases in migration and invasiveness in vitro as well as experimental metastasis in vivo. These preclinical findings may provide a plausible scientific basis for clinical observations of prolonged OS by suppression of further spread of metastasis in breast cancer patients treated with eribulin.

Breast cancers can be classified into oestrogen receptors (ERs)+ human epithelial growth receptor 2 (HER2)+ and so-called 'triple negative' breast cancer (TNBC; negative for ER, HER2, and progesterone receptors) subtypes. Both ER+ and HER2+ tumours have luminal epithelial characteristics, whereas a large fraction of triple negative tumours have stem cell/basal-like properties (Perou et al, 2000; Nielsen et al, 2004; Neve et al, 2006; Shipitsin et al, 2007). In the last decade considerable progress has been made in the treatment of ER+ and HER2+ tumours, with multiple types of therapies now available including hormonal and monoclonal antibody-based therapies and small molecule inhibitors of tyrosine kinases for both localised and metastatic disease (Arteaga et al, 2012). Consequently, survival rates of breast cancer patients with luminal subtypes have improved significantly, especially for early-stage disease. In contrast, TNBC, which comprises 10–15% of all breast cancers, still lacks effective targeted therapies which, when combined with its typically heterogeneous histology and propensity for early metastasis, results in poor 5-year survival rates for this breast cancer subtype (Carey et al, 2007; Lehmann et al, 2011; Shah et al, 2012). Given this situation, preventing metastatic spread and treatment of existing metastatic disease in TNBC remain among the top challenges in breast cancer treatment today.

Eribulin (Halaven) is a non-taxane inhibitor of microtubule dynamics that exerts its primary pharmacologic effects by preventing normal mitotic spindle formation, leading to irreversible mitotic blockage and subsequent cell death by apoptosis (Towle et al, 2001; Kuznetsov et al, 2004; Okouneva et al, 2008; Towle et al, 2012). Eribulin binds to the plus ends of microtubules (Smith et al, 2010), resulting in a pattern of microtubule dynamics inhibition that is distinct from those of other clinically used tubulin agents including epothilones, vinca alkaloids, and taxanes. Eribulin is currently approved for clinical use in many countries worldwide, including United States, Japan, and EU countries for treatment of certain patients with advanced breast cancer. For instance, in the United States and EU, eribulin is approved for patients with locally invasive or metastatic breast cancer who have previously received at least two chemotherapeutic regimens for metastatic disease, including an anthracycline and a taxane (Cortes et al, 2011). Interestingly, two different phase 3 clinical trials in metastatic breast cancer patients have suggested that eribulin has more pronounced effects on overall survival (OS) compared with progression-free survival (PFS) (Cortes et al, 2011). One possible explanation for this clinical observation is that eribulin may suppress the incidence of new metastasis, thus providing an increased survival benefit to patients even under conditions in which the primary tumour and preexisting metastatic tumour may progress. The preclinical studies described herein were designed to assess whether eribulin might have such anti-metastatic properties, based on reversion of the metastasis-promoting process termed as epithelial–mesenchymal transition (EMT).

Epithelial–mesenchymal transition and its reverse process, mesenchymal–epithelial transition (MET), were originally identified as playing central roles during early embryonic development (Yang and Weinberg, 2008). More recently, EMT has been shown to be a key metastasis-promoting step in many cancers (Gavert and Ben-Ze'ev, 2008). In tumours, gain of mesenchymal characteristics and loss of epithelial characteristics via EMT correlate well with tumour progression, maintenance, drug resistance, and metastasis (Polyak and Weinberg, 2009; Gunasinghe et al, 2012). Epithelial–mesenchymal transition progression is characterised by loss of the epithelial marker E-cadherin, together with increased expression of mesenchymal markers such as N-cadherin and vimentin. During metastatic progression, EMT drives primary epithelial-like tumour cells to acquire invasive mesenchymal phenotypes, with increased motility and invasiveness, triggering dissemination from the tumour and infiltration into the tumour vascular. These EMT-

driven cells then circulate in the blood flow, and subsequently redifferentiate via MET during colonisation and growth at distant metastatic sites (Bonnomet et al, 2012; Yu et al, 2013). Thus, considering EMT's role at the onset of the metastatic process, controlling EMT in tumours is now considered to be a promising strategy to inhibit metastasis and improve survival of cancer patients.

In the present study, we investigated potential relationships between EMT/MET balance altered with eribulin treatment, as measured in preclinical TNBC models, and eribulin's apparent ability to prolong OS in TNBC patients without corresponding increases in PFS. In aggregate, these results suggest that eribulin triggers a phenotypic shift in balance from the more aggressive EMT state to a less aggressive MET state, the latter being associated with decreased potential for metastasis and invasion.

MATERIALS AND METHODS

Compounds. Eribulin mesilate was chemically synthesised at Eisai Co., Ltd (Tsukuba, Japan). 5-Fluorouracil (5-FU) was obtained from Sigma-Aldrich (St Louis, MO, USA).

Cell culture. MX-1 was obtained from the United States National Cancer Institute. Hs578T, MDA-MB-157, and MCF10A were purchased from American Type Cell Collection. MX-1 was maintained in RPMI-1640 medium supplemented with 10% fetal bovine serum. Hs578T was maintained in DMEM supplemented with 10% fetal bovine serum and $10 \mu g \, ml^{-1}$ insulin. MDA-MB-157 was maintained in McCoy's 5A medium supplemented with 10% fetal bovine serum. MCF10A was cultured in DMEM/F12 medium supplemented with 5% horse serum, $10 \mu g \, ml^{-1}$ insulin, $20 \, ng \, ml^{-1}$ EGF, $500 \, ng \, ml^{-1}$ hydrocortisone, and $100 \, ng \, ml^{-1}$ cholera toxin. Recombinant TGF-β was purchased from R&D (Minneapolis, MN, USA).

Proliferation assay. Cells were plated in 96-well plates and cultured with indicated concentration of compounds for 3 days, followed by cell number and viability determinations as measured by CellTiter-Glo Luminescent Cell Viability Assay (Promega, Madison, WI, USA).

Gene expression analysis. Total RNA from cultured cells treated with eribulin for 7 days was isolated using the RNeasy Mini kit (Qiagen, Valencia, CA, USA). Reverse transcription was carried out using the High Capacity cDNA Reverse Transcription kit (Life Technologies, Grand Island, NY, USA). Synthesised cDNA was amplified with Taqman probes and quantities of DNA were measured by ABI7900 (Applied Biosystems, Life Technologies). Assessment of changes in gene expression was conducted by comparison of delta delta Ct values for each sample. TaqMan probes used in this study are summarised in Supplementary Table 1.

Western blotting analysis. The cultured cells were lysed with Pierce RIPA Buffer (Thermo Scientific, Waltham, MA, USA) with Halt protease inhibitor Cocktail (Thermo Scientific). Lysates mixed with sample buffer were electrophoretically separated and transferred onto membranes. Membranes were blocked with 5% skim milk, followed by incubations with anti-human E-cadherin antibody (24E10; Cell Signaling Technology, Danvers, MA, USA), anti-human N-cadherin antibody (#610920; BD Biosciences, San Jose, CA, USA), anti-human vimentin antibody (D21H3; Cell Signaling Technology), anti-human Smad2/3 (#07-408; Millipore, Billerica, MA, USA), anti-human phospho-Smad2 (Ser465/467) (#AB3849; Millipore), anti-human phospho-Smad3 (Ser423/425) (#07-1389; Millipore), and anti-human β-actin antibody (#4963; Cell Signaling Technology). After washing with TBS-0.05% Tween, membranes were incubated with HRP-conjugated anti-mouse or

anti-rabbit IgG. After washing with TBS-0.05% Tween, membranes were incubated with ECL Prime Western Blotting Detection Reagent (GE Healthcare, Little Chalfont, UK). Signals were detected and analysed using a Luminescent Image Analyzer LAS-4000 (Fuji Film, Tokyo, Japan). Signals were detected and analysed using a Luminescent Image Analyzer LAS-4000 (Fuji Film).

In vivo tumour xenograft growth assay and sample preparation for in vivo immunohistochemical analyses. For in vivo xenograft specimens, 10×10^6 MX-1 cells in a Matrigel suspension were subcutaneously injected into the right flank of athymic mice (CAnN.Cg-Foxn1nu/CrlCrlj; Charles River Laboratories Japan, Yokohama, Japan). Nine to eleven days after inoculation, eribulin (0.3, 1, and 3 mg kg^{-1}) or vehicle was intravenously administrated; this was defined as day 1. On days 4 or 8, mice were killed, and tumours were isolated and measured. Collected tumours were fixed in 10% neutral buffered formalin solution (Wako Pure Chemical Industries, Osaka, Japan) for 24 h followed by embedding in Tissue-Tek VIP 5 Jr. (Sakura, Torrance, CA, USA).

Immunohistochemical analysis. Sections (5 μm) of formalin-fixed, paraffin-embedded tumours prepared as above were made using a rotary microtome (Leica Biosystems, Wetzlar, Germany, RM2255). Sections were placed on charged slides and dried on a warm plate at 35–37 °C overnight. Immunohistochemistry (IHC) staining using anti-E cadherin (#3195; Cell Signaling Technology), anti-ZEB1 (#NBP1-05987; Novus Biologicals, Littleton, CO, USA), and anti-N-cadherin (#ab18203; Abcam) primary antibodies was performed on either a Leica BOND-MAX Autostainer (Leica Biosystems) or a Leica ST5020 Multistainer (Leica Biosystems). Stained mounted slides were digitised using a ScanScope XTTM (Aperio Technologies, Vista, CA, USA) whole slide automated scanning system. Image analysis and quantification of IHC staining was performed using Aperio ImageScope software version 11.1.2.760 (Aperio Technologies). Regions of interest (ROIs) for quantification were defined as the entire tumour cross-sectional areas of each sample (one ROI per sample). The following Aperio image analysis algorithms were used to quantify IHC staining within ROIs: IHC nuclear (quantification of ZEB1), IHC membrane (quantification of E-cadherin), and colocalisation (quantification of N-cadherin).

In vitro migration and invasion assay. BioCoat Matrigel invasion chambers, 24-well plates (BD Biosciences) were utilised. For the cell migration assay and the invasion assay, 5×10^3 and 2.5×10^3 cells, respectively, were seeded onto the porous membranes in upper chambers of BioCoat control cell-culture inserts (8.0 μm pore size; BD Biosciences) after treatment for 7 days with eribulin or 5-FU. Top chambers (culture inserts) were filled with serum-free medium, and bottom chambers were filled with medium containing 20% FBS as a chemoattractant. After 16 h incubation for migration or 26 h incubation for invasion, the number of cells that had migrated to bottom surfaces of the membranes was counted after staining with Geimsa solution. Numbers of cells in wells were calculated using means from five randomly selected fields.

Lung metastasis model. MX-1 cells were pretreated with 1 nM eribulin, 3 μM 5-FU, or DMSO as a control for 7 days. CB17-SCID mice (Charles River Laboratories Japan) were pretreated with cyclophosphamide to eliminate residual immune cells by intraperitoneal injection of 150 mg kg^{-1} per day for 2 days (Shankar et al, 2007), followed by intravenous tail vein injection of 1×10^6 MX-1 cells. Thirteen days after injection, lungs were harvested and stained with Bouin's solution to visualise metastatic colonies. For survival analysis, mice were monitored daily for signs of morbidity, including body weight, hydration level, coat appearance, mobility, and behaviour. Mice that showed cumulative signs meeting the criteria of a moribund state were euthanised. All procedures using laboratory animals were done in accordance with all applicable

institutional and government regulatory guidelines and policies were performed in an animal facility accredited by the Center for Accreditation of Laboratory Animal Care of the Japan Health Sciences Foundation.

Statistical analysis. Eribulin-treated vs control groups were analysed by the Dunnett multiple comparisons test using two-sided approaches. Values of $P < 0.05$ were considered as statistically significant. Statistical analyses were performed using GraphPad Prism version 5.04 (GraphPad Software, La Jolla, CA, USA) or R (v2.15.2, http://www.r-project.org/index.html) and SAS (v9.2 2M2, Cary, NC, USA) programs. Analyses of lung metastatic nodules and survival data were done using Kaplan–Meier and log-rank test methods and the Mann–Whitney U-test (GraphPad Prism version 6, La Jolla, CA, USA).

RESULTS

Eribulin reverses EMT and induces MET in TNBC cells in vitro. To investigate the effects of eribulin on EMT/MET balance, three TNBC cell lines were treated with eribulin for 7 days (Figure 1A). The doses of eribulin for MX-1 and Hs578T were IC$_{50}$ and three times IC$_{50}$ decided by 3 days proliferation assay result (Supplementary Figure S1A). For MDA-MB-157, half IC$_{50}$ and IC$_{50}$ of eribulin were selected because almost all cells died after 7 days treatment with three times IC$_{50}$. Although eribulin strongly inhibited proliferation of these cells, surviving cells were no longer spindle shaped like control cultures, but instead had flat, more epithelial-like morphologies (Figure 1B). This conversion from mesenchymal to epithelial-like morphologies prompted us to examine alterations in EMT/MET-related genes. RNA from surviving TNBC cells treated with eribulin for 7 days was assayed by qPCR analysis. As shown in Figure 1C (MX-1), Figure 1D (MDA-MB-157), and Figure 1E (Hs578T), eribulin treatment consistently upregulated mRNA expression levels of epithelial markers CDH1 and KRT18, while it downregulated mesenchymal markers CDH2, VIM, TWIST1, SNAI2, ZEB1, and ZEB2, even though the pattern and degree of these alterations was somewhat different among the three TNBC cell lines (Figure 1C, D and E). Of the three, eribulin effects on EMT/MET markers were most robust in MX-1 cells, so this line was selected for further, more detailed analyses. Thus, using MX-1 cells, western blotting analysis confirmed that protein levels of key EMT/MET markers behaved similarly to mRNA expression patterns: eribulin increased levels of E-cadherin protein while decreasing levels of N-cadherin and vimentin proteins (Figure 1F and G). Taken together, results of morphological observations and gene and protein expression patterns strongly point to eribulin-induced reversion of EMT and induction of MET in TNBC cells.

Eribulin reverses EMT and induces MET in MX-1 TNBC tumour xenografts in mice. Next, eribulin's ability to induce a shift from EMT to MET phenotypes was tested in MX-1 tumour xenografts in vivo. MX-1 cells were transplanted into athymic mice to establish MX-1 xenografts, followed by treatment of animals with eribulin using the schedule shown in Figure 2A. Under these conditions, eribulin showed a significant antitumour activity as determined by measurement of tumour weights on days 4 and 8 of the study (Supplementary Table 2). Nevertheless, even in tumours in the 3 mg kg^{-1} eribulin group, residual tumour tissues remained intact and showed evidence of tumour vasculature remodelling (Matsui et al, 2013; Funahashi et al, manuscript in preparation). Therefore, an IHC analysis of EMT/MET-related proteins in the resected tumours was performed. Figure 2B showed representative images of IHC staining for E-cadherin, N-cadherin, and ZEB1 protein in tumours from animals receiving each of the three eribulin treatment dose levels. As shown, in all eribulin-treated
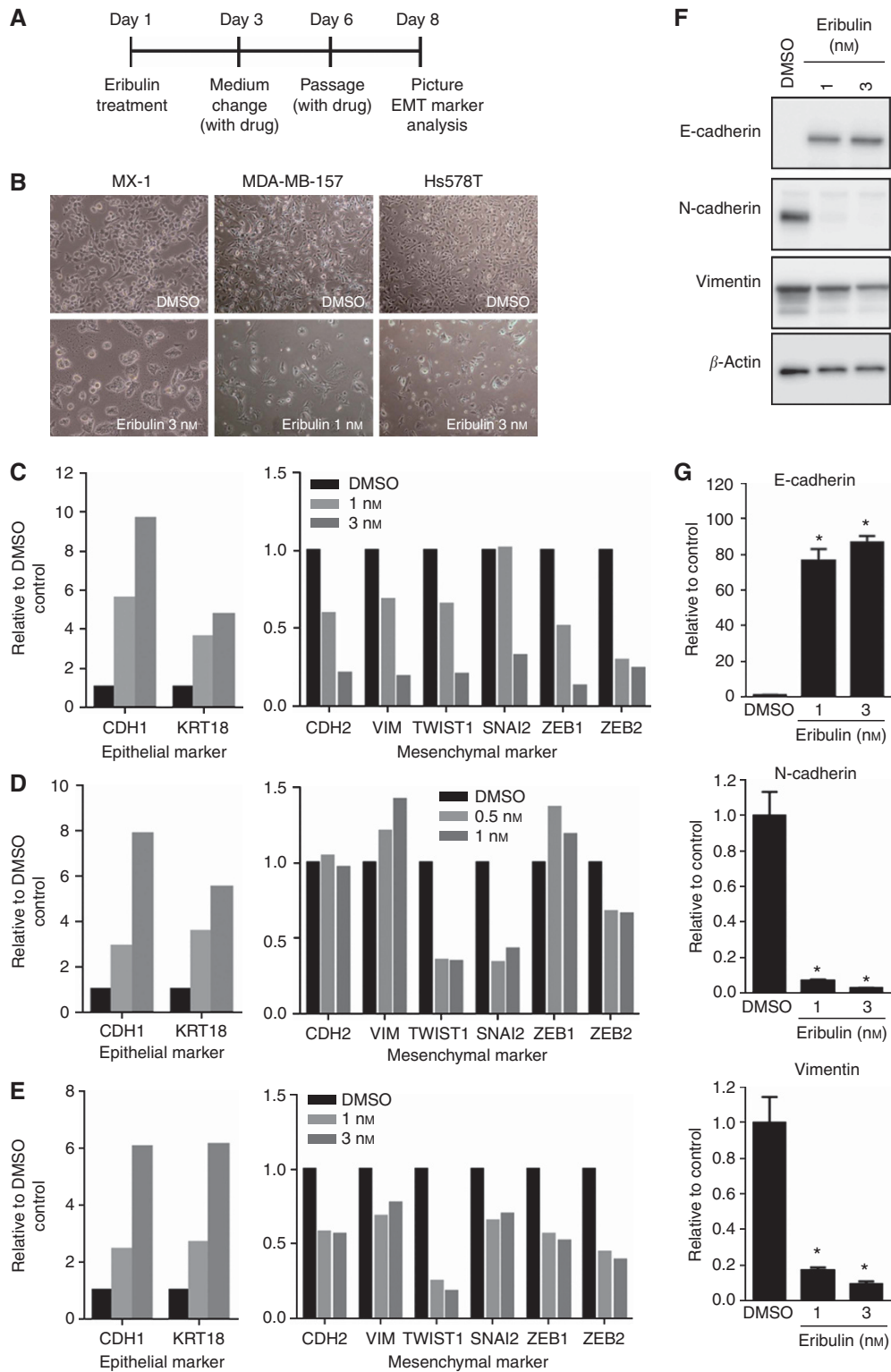
Figure 1. Eribulin treatment of TNBC breast cancer cells *in vitro* eribulin reverses EMT and induces MET. (**A**) Schematic representation of treatment scheme. (**B**) Representative images of TNBC cells following treatment with indicated dose of eribulin for 1 week. Images taken at ×10 magnification. (**C–E**) Expression levels of EMT/MET-related marker genes in eribulin-treated (**C**) MX-1, (**D**) MDA-MB-157, and (**E**) Hs578T TNBC cells as measured by qPCR. Gene expression levels were normalised to GAPDH expression. (**F**) Protein expression of E-cadherin, N-cadherin, and vimentin as assessed by immunoblot analysis. β-Actin was used as a loading control. (**G**) Quantification of protein levels of E-cadherin (upper), N-cadherin (middle), and vimentin (lower) from the immunoblot analysis of (**G**). Bars show mean ± s.e.m. ($n = 3$). *$P < 0.05$ *vs* control group (Dunnett multiple comparison test).

groups, the epithelial E-cadherin signal was increased whereas the mesenchymal N-cadherin and ZEB1 signals were decreased. Quantification of these IHC results for all animals in each group

revealed that these alterations were significant at all doses tested when compared with the corresponding vehicle controls (Figure 2C). Together with results from cell-based studies, analysis
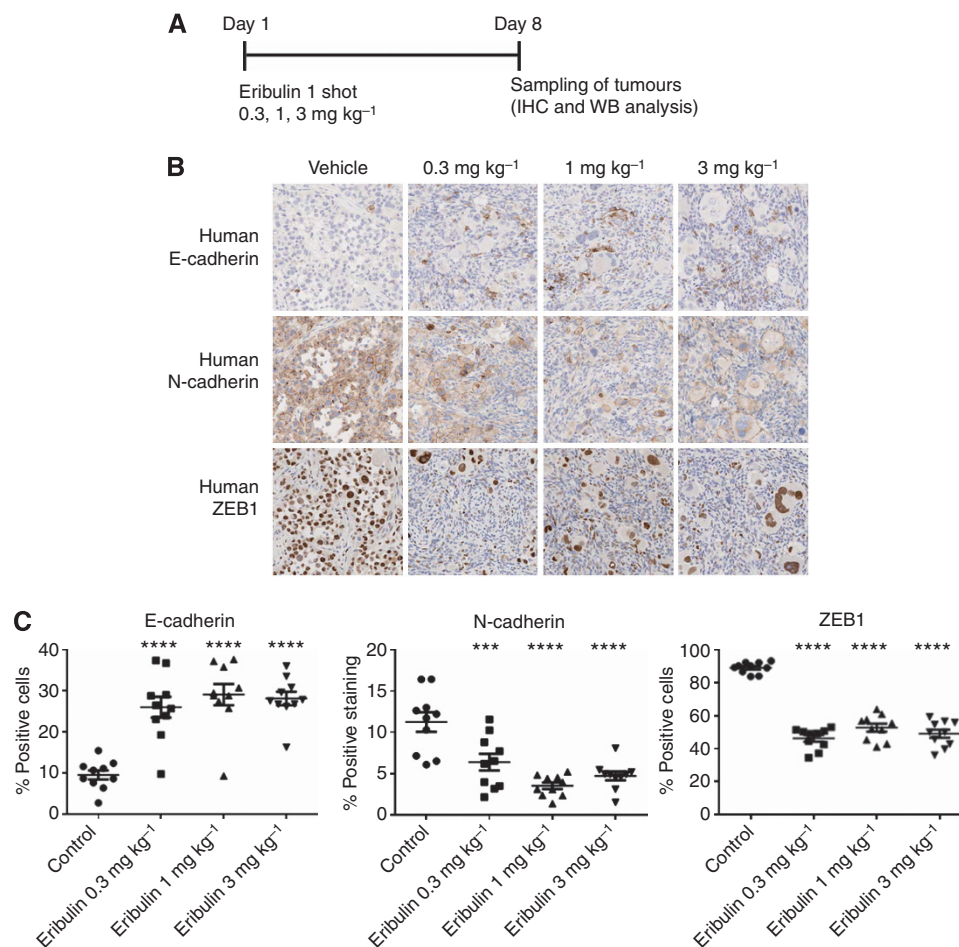
Figure 2. Eribulin reverses EMT and induces MET in MX-1 breast cancer xenografts *in vivo*. (**A**) Schematic representation of treatment scheme. (**B**) Representative IHC images of E-cadherin (upper), N-cadherin (middle), and ZEB1 (lower) in tumour specimens from animals treated with 0.3, 1, and 3 mg kg^{-1} eribulin. Images taken at ×100 magnification. (**C**) Quantification of IHC staining of the markers shown in (**B**). Data for individual tumours are presented as points, with means ± s.e.m. of the group shown by lines ($n = 10$). ***$P < 0.001$, ****$P < 0.0001$ *vs* control group (Dunnett-type multiple comparison test).

of protein expression levels in *in vivo* MX-1 tumour xenografts provides strong evidence for eribulin-induced reversion of EMT and induction of MET in breast cancer cells.

Eribulin regulates TGF-β signalling pathway via downregulation of Smad phosphorylation. To examine the mechanism by which eribulin induces MET in cells, the effect of eribulin on TGF-β/Smad signalling, a key signalling pathway for induction of EMT, was investigated. It is known that TGF-β enhances phosphorylation of receptor-regulated Smad2 and Smad3 proteins, resulting in enhanced complexing with Smad4. Translocation of the resulting complex into the nucleus activates transcription of essential EMT-related genes, including TWIST1, SNAI1, SNAI2, ZEB1, and others (Takano *et al*, 2007; Gregory *et al*, 2011). To evaluate the effect of eribulin on this pathway, MCF10A normal mammary epithelial cells were utilised. These cells represent a non-cancerous, triple negative basal cell type and as such are often used as an EMT model since they quickly undergo EMT in response to TGF-β. Figure 3A shows the treatment scheme of the experiment. The EMT phenotype of MCF10A cells treated with TGF-β for 7 days was confirmed by cell morphology (Figure 3B) as well as gene expression profiles of epithelial and mesenchymal markers (Figure 3C). Next, effects of eribulin on MCF10A cells already induced to the EMT phenotype by TGF-β treatment were examined. For this analysis, eribulin treatment was begun after cells had been induced to the EMT phenotype by 7 days of TGF-β

pretreatment, and 7 days later cellular morphology and gene expression profiles were examined. The concentration of eribulin used in this experiment was ∼$0.5 \times$ IC$_{50}$, 0.25 nM (see Supplementary Figure S1B). As shown in Figure 3D on day 15, eribulin treatment reversed the observed phenotype from the previously induced spindle-like EMT morphology seen at day 8 to the original cuboidal morphology typical of TGF-β-untreated cells (compare Figure 3D, right, with Figure 3B, left). Furthermore, eribulin treatment also significantly upregulated mRNA expression levels of epithelial marker CDH1, while downregulating several mesenchymal markers (Figure 3E). Finally, phosphorylation levels of Smad2 and Smad3 were investigated. MCF10A cells were pretreated with eribulin for 1 day, and the phosphorylation status of Smad2 and Smad3 was analysed 1 h after subsequent TGF-β stimulation. As shown in Figure 3F, eribulin pretreatment significantly decreased TGF-β-induced phosphorylation of Smad2 and Smad3, suggesting that the MET induced by eribulin was, at least in part, due to of downregulation of the TGF-β/Smad pathway.

Eribulin decreases migration and invasion capacity of MX-1 TNBC cell *in vitro*. One of the functional changes associated with EMT is an increase in migration and invasion capacities, traits typically associated with mesenchymal phenotypes. To investigate whether decreases in cell migration and invasion capacities accompany the eribulin-induced shift from EMT to MET
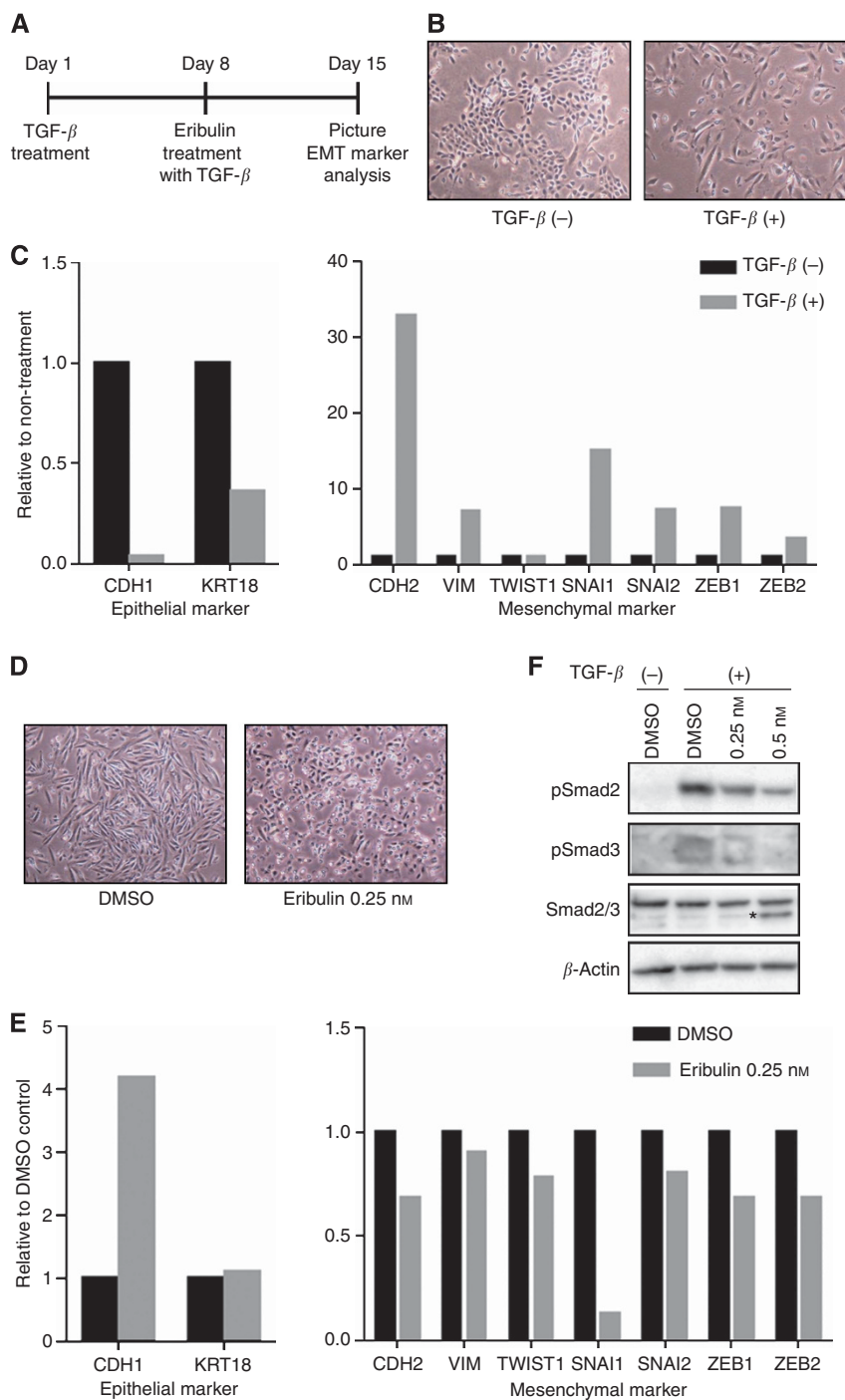
Figure 3. Eribulin downregulates TGF-β/Smad pathway. (**A**) Schematic representation of TGF-β and eribulin treatment schedules for studies shown in (**B–E**). (**B**) Representative day 8 images of MCF10A cells following 7 days treatment with TGF-β (10 ng ml^{-1}). Images taken at $\times$10 magnification. (**C**) Expression levels of EMT-related markers in MCF10A cells treated with TGF-β (10 ng ml^{-1}) at day 8 as measured by qPCR. Gene expression levels were normalised to GAPDH expression. (**D**) Representative day 15 images of MCF10A cells preinduced to the EMT phenotype by TGF-β pretreatment, followed by additional 7 days treatment with eribulin. Images taken at $\times$10 magnification. (**E**) Expression levels of EMT-related markers in the same eribulin-treated MCF10A cells as in (**D**), as measured by qPCR. (**F**) Immunoblot analysis of phosphorylated Smad2, phosphorylated Smad3, and total Smad2/3 in MCF10A cells pretreated with 0.25 nM eribulin for 1 day followed by TGF-β treatment for 1 h. β-Actin was used as a loading control. * indicates non-specific band.

phenotypes seen above, *in vitro* migration and invasion assays were conducted. For these studies, MX-1 cells were treated for 7 days with 1 or 3 nM eribulin, or 10 μM 5-FU (active metabolite of capecitabine, the comparator used in a recent phase III clinical trial of eribulin; see Kaufman *et al*, 2012), followed by drug washout and evaluation of *in vitro* migration and invasion in the absence of drugs (Figure 4A). The concentration of 5-FU used, 10 μM, was

approximately a 2$\times$ IC$_{50}$ growth inhibitory concentration (Supplementary Figure S1C). Treatment with eribulin significantly decreased both the migration (Figure 4B and C) and invasiveness (Figure 4D and E) capacities of MX-1 cells *in vitro*. In contrast, although treatment with 5-FU also decreased both migration and invasiveness of MX-1 cells, such effects were smaller than those seen with eribulin (Figure 4B–E).
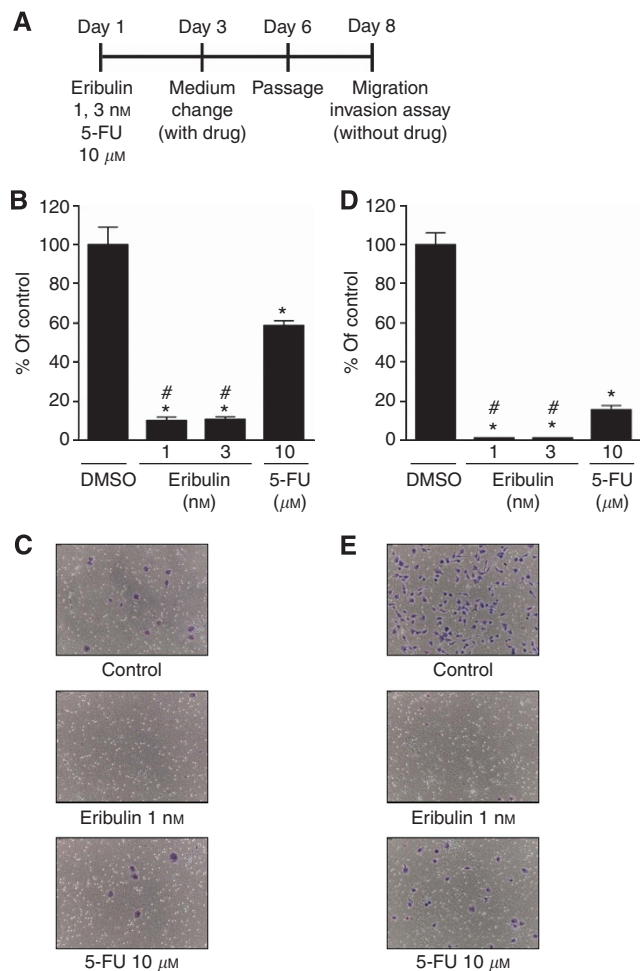
Figure 4. Eribulin treatment of MX-1 breast cancer cells *in vitro* decreases migration and invasiveness capacities. (**A**) Schematic representation of treatment scheme. (**B**) Inhibitory effects of eribulin or 5-FU on migration of MX-1 cells, expressed as percent changes in eribulin or 5-FU-treated cells compared with migration seen with untreated control cells. Data represent means ± s.e.m. from three independent experiments. *$P < 0.05$ *vs* vehicle control (Dunnett multiple comparison test). #$P < 0.05$ *vs* 5-FU 10 μM (the Dunnett multiple comparison test except control). (**C**) Representative fields in the migration assay ($\times$ 20 magnification). (**D**) Inhibitory effects of eribulin or 5-FU on invasion of MX-1 cells, expressed as percent changes in eribulin or 5-FU-treated cells compared with invasion seen with untreated control cells. Data represent means ± s.e.m. from three independent experiments. *$P < 0.05$ *vs* vehicle control (Dunnett multiple comparison test). #$P < 0.05$ *vs* 5-FU 10 μM (the Dunnett multiple comparison test except control). (**E**) Representative fields in the invasion assay ($\times$ 20 magnification).

Eribulin treatment decreases lung metastases and prolongs survival in MX-1 *in vivo* experimental metastasis model. Finally, we utilised an *in vivo* experimental metastasis model to investigate whether MX-1 cells pretreated with eribulin have a reduced capacity to generate metastatic lung nodules, and whether the host mice would survive longer. Equivalent numbers of MX-1 cells pretreated *in vitro* with DMSO, 1 nM eribulin, or 3 μM 5-FU for 7 days were injected into tail veins of mice, followed 13 days later by assessment of the number of metastatic lung nodules. To exclude the possibility that pretreated cells had lost their viability at the time of injection, proliferation rates of samples of pretreated cells (i.e., cells identical to those injected into mice) were measured after washout of the drugs. Results indicated that the post-washout
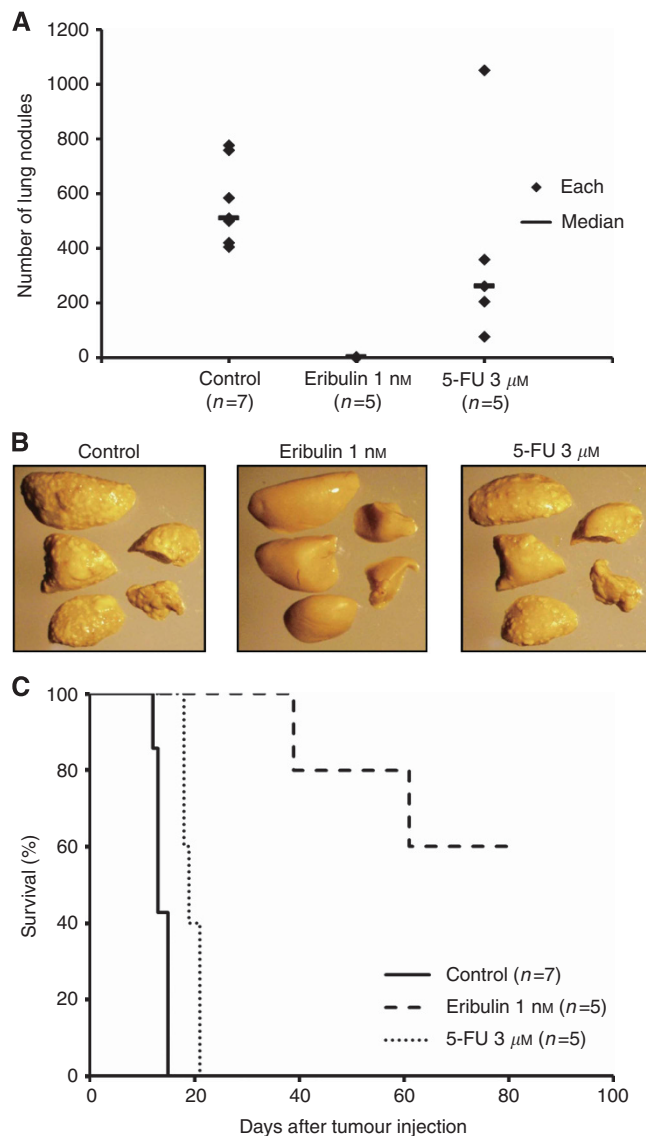

Figure 5. Eribulin treatment reduces metastasis and increases survival in MX-1 *in vivo* experimental metastasis model. (**A**) Numbers of lung nodules at day 15 after tail vein injection of MX-1 cells that had been pretreated with eribulin, 5-FU, or DMSO ($n = 5$–7). *$P < 0.01$ by Kruskal–Wallis Dunn's multiple comparison test. (**B**) Representative lung images ($\times$ 20 magnification) at day 15 after cell injection. (**C**) Survival of animals in the experimental metastasis assay ($n = 5$–7).

proliferation rates of both eribulin- and 5-FU-pretreated cells were slightly slower at 2 days, but had recovered to virtually identical rates as DMSO control cells by day 4, indicating that all post-washout cells injected into tail veins retained full viability and proliferative capacity (Supplementary Figure S2). Thirteen days after tail vein injection, numbers of metastatic lung nodules were assessed. As shown in Figure 5A and B, animals injected with MX-1 cells pretreated with eribulin showed dramatic reductions in the number of metastatic lung nodules compared with controls. Pretreatment of MX-1 cells with 5-FU also led to a reduction in numbers of metastatic lung nodules compared with controls (Figure 5A and B), albeit to a considerably lesser degree than seen with eribulin. Next, we examined whether the observed reductions in lung metastases were associated with prolonged survival. As shown in Figure 5C, control mice started to die around 13 days after DMSO-treated MX-1 cell injection, with mice in the 5-FU group starting to die only a few days later. By day 21, all mice in

both the DMSO and 5-FU groups had died. In marked contrast, the first deaths in the eribulin-treated group were not seen until day 39, with the final survival rate at the conclusion of the study on day 80 being 60% (Figure 5C), linking the reduction in metastases to functional prolongation of survival.

DISCUSSION

Recent advances in novel drug development strategies have improved treatment paradigms for hormone-sensitive and HER2 overexpressing breast cancers; however, the most malignant and heterogeneous subtype, TNBC, remains largely intractable due to an aggressive metastatic character and rapid recurrence after treatment. Emerging results from many groups suggest that TNBC's resistance to chemotherapy may be explained in part by the EMT hypothesis. Epithelial–mesenchymal transition progression is characterised by a transition from epithelial to mesenchymal phenotype, loss of proteins involved in cell junctions, such as E-cadherin, and increased expression of mesenchymal markers such as N-cadherin and vimentin. Moreover, circulating tumour cells (CTCs) involved in breast cancer metastasis are reported to harbour mesenchymal characteristics (Yu et al, 2013), and gene signatures of mesenchymal type cells induced by EMT are highly correlated with those of cancer stem cells (Shipitsin et al, 2007; Mani et al, 2008; Taube et al, 2010). Thus, the processes of tumour aggressiveness, chemoresistance, metastasis, and invasion appear to be inextricably linked to EMT.

The current preclinical studies represent an attempt to identify the scientific basis behind clinical observations of eribulin's enhancement of OS without corresponding increases in PFS. The studies described here have uncovered a potential new biology associated with eribulin treatment, regulation of tumour EMT/MET balance, which may add a new dimension to eribulin's known antimitotic, antiproliferative effects on cancer cells. Results in support of this conclusion are several-fold. First, in TNBC cells in vitro, eribulin promoted a shift from EMT to MET states, as shown by phenotypic shifts from mesenchymal to epithelial morphologies, as well as changes in EMT/MET-related markers strongly favouring MET. Second, eribulin treatment of mice bearing TNBC xenografts led to increased tumour expression of epithelial markers concurrent with decreased levels of mesenchymal markers. Third, eribulin treatment of TNBC cells in vitro led to decreased cellular migration and invasiveness capacities, an observation consistent with the known functional phenotype of MET. Finally, eribulin pretreated TNBC cells had a significantly decreased capacity to colonise the lung in an in vivo experimental metastasis model, findings that also correlated with significant prolongation of survival.

It has been shown in several reports that the primary target of eribulin is tubulin and microtubules (Towle et al, 2001; Kuznetsov et al, 2004; Jordan et al, 2005; Okouneva et al, 2008; Smith et al, 2010). However, the relationship between microtubule regulation and EMT has received little attention. Smad proteins, which are essential mediators of TGF-β signalling pathway, normally bind microtubules in the absence of TGF-β but dissociate from them upon TGF-β stimulation (Dong et al, 2000). Dissociated Smad2 and Smad3 become phosphorylated and then associate with Smad4, followed by translocation of the entire complex to the nucleus where it activates transcription. Eribulin inhibits the growth phase of microtubule dynamics (Jordan et al, 2005), by binding to high affinity sites on microtubule plus ends (Smith et al, 2010), possibly resulting in maintenance of the association between Smad proteins and microtubules with consequent inhibition of Smad phosphorylation. In fact, the microtubule stabiliser paclitaxel, even with a distinct mode of action from eribulin, decreased Smad2 phosphorylation in gastric cancer (Tsukada et al, 2013). On the other hand, the microtubule destabiliser nocodazole enhances the release of Smad proteins from microtubules and thus increases their phosphorylation (Dong et al, 2000). Although it cannot be excluded that eribulin may have other unique targets to evoke MET, the precedents set by paclitaxel and nocodazole in altering Smad-related signalling suggests that eribulin binding to microtubules may at least partially explain its induction of MET in TNBC cells as observed in our studies.

Involvement of EMT in drug resistance has been reported in several cancer types. For instance, positive staining for the mesenchymal marker Vimentin appears in specimens from non-small cell lung cancer (NSCLC) patients who develop resistance to EGFR inhibitors, suggesting that EMT has been triggered in such tumours (Uramoto et al, 2010; Chung et al, 2011; Sequist et al, 2011). It will be interesting to determine whether eribulin reverses the EMT phenotype of lung cancer cells preclinically to reduce resistance to EGFR inhibitors. An important caveat to the studies presented here is that it is not currently known whether other tubulin-targeting agents, such as the taxanes, vinca alkaloids, or epothilones, have effects on EMT/MET balance similar to those described here for eribulin. Studies are currently ongoing to investigate this important question.

In conclusion, the preclinical studies presented here reveal that, in addition to having a primary anticancer mechanism associated with classical antimitotic effects, eribulin may also render residual tumours less aggressive and less likely to metastasise by triggering a shift from mesenchymal to epithelial phenotypes via reversal of the EMT state to the MET state.

ACKNOWLEDGEMENTS

CONFLICT OF INTEREST

All authors are employees of Eisai Co., Ltd, or Eisai Inc.

REFERENCES

Arteaga CL, Sliwkowski MX, Osborne CK, Perez EA, Puglisi F, Gianni L (2012) Treatment of HER2-positive breast cancer: current status and future perspectives. Nat Rev Clin Oncol 9(1): 16–32.

Bonnomet A, Syne L, Brysse A, Feyereisen E, Thompson EW, Noel A, Foidart JM, Birembaut P, Polette M, Gilles C (2012) A dynamic in vivo model of epithelial-to-mesenchymal transitions in circulating tumor cells and metastases of breast cancer. Oncogene 31(33): 3741–3753.

Carey LA, Dees EC, Sawyer L, Gatti L, Moore DT, Collichio F, Ollila DW, Sartor CI, Graham ML, Perou CM (2007) The triple negative paradox: primary tumor chemosensitivity of breast cancer subtypes. Clin Cancer Res 13(8): 2329–2334.

Chung JH, Rho JK, Xu X, Lee JS, Yoon HI, Lee CT, Choi YJ, Kim HR, Kim CH, Lee JC (2011) Clinical and molecular evidences of epithelial to mesenchymal transition in acquired resistance to EGFR-TKIs. Lung Cancer 73(2): 176–182.

Cortes J, O'Shaughnessy J, Loesch D, Blum JL, Vahdat LT, Petrakova K, Chollet P, Manikas A, Dieras V, Delozier T, Vladimirov V, Cardoso F, Koh H, Bougnoux P, Dutcus CE, Seegobin S, Mir D, Meneses N, Wanders J, Twelves C, investigators E (2011) Eribulin monotherapy versus treatment of physician's choice in patients with metastatic breast cancer (EMBRACE): a phase 3 open-label randomised study. Lancet 377(9769): 914–923.

Dong C, Li Z, Alvarez Jr R, Feng XH, Goldschmidt-Clermont PJ (2000) Microtubule binding to Smads may regulate TGF beta activity. *Mol Cell* **5**(1): 27–34.

Gavert N, Ben-Ze'ev A (2008) Epithelial-mesenchymal transition and the invasive potential of tumors. *Trends Mol Med* **14**(5): 199–209.

Gregory PA, Bracken CP, Smith E, Bert AG, Wright JA, Roslan S, Morris M, Wyatt L, Farshid G, Lim YY, Lindeman GJ, Shannon MF, Drew PA, Khew-Goodall Y, Goodall GJ (2011) An autocrine TGF-beta/ZEB/miR-200 signaling network regulates establishment and maintenance of epithelial-mesenchymal transition. *Mol Biol Cell* **22**(10): 1686–1698.

Gunasinghe NP, Wells A, Thompson EW, Hugo HJ (2012) Mesenchymal-epithelial transition (MET) as a mechanism for metastatic colonisation in breast cancer. *Cancer Metastasis Rev* **31**(3-4): 469–478.

Jordan MA, Kamath K, Manna T, Okouneva T, Miller HP, Davis C, Littlefield BA, Wilson L (2005) The primary antimitotic mechanism of action of the synthetic halichondrin E7389 is suppression of microtubule growth. *Mol Cancer Ther* **4**(7): 1086–1095.

Kaufman PA, Awada A, Twelves C, Yelle L, Perez E, Wanders J, Olivo MS, He Y, Dutcus CE, Cortes J (2012) A Phase III, open-label, randomized, multicenter study of eribulin mesylate versus capecitabine in patients with locally advanced or metastatic breast cancer previously treated with anthracyclines and taxanes. *San Antonio Breast Cancer Symposium;* San Antonio, TX, USA; p S6-6.

Kuznetsov G, Towle MJ, Cheng H, Kawamura T, TenDyke K, Liu D, Kishi Y, Yu MJ, Littlefield BA (2004) Induction of morphological and biochemical apoptosis following prolonged mitotic blockage by halichondrin B macrocyclic ketone analog E7389. *Cancer Res* **64**(16): 5760–5766.

Lehmann BD, Bauer JA, Chen X, Sanders ME, Chakravarthy AB, Shyr Y, Pietenpol JA (2011) Identification of human triple-negative breast cancer subtypes and preclinical models for selection of targeted therapies. *J Clin Invest* **121**(7): 2750–2767.

Mani SA, Guo W, Liao MJ, Eaton EN, Ayyanan A, Zhou AY, Brooks M, Reinhard F, Zhang CC, Shipitsin M, Campbell LL, Polyak K, Brisken C, Yang J, Weinberg RA (2008) The epithelial-mesenchymal transition generates cells with properties of stem cells. *Cell* **133**(4): 704–715.

Matsui J, Toyama O, Ino M, Semba T, Uesugi M, Muto H, Oestreicher JL, Takahashi K, Matsuura K, Sato Y, Uehara T, Kimura T, Watanabe H, Ozawa Y, Asano M, Adachi Y, Aoshima K, Funahashi Y (2013) Eribulin caused re-modeling of tumor vasculature altering gene expression profiling in angiogenesis and Epithelial Mesenchymal Transition (EMT) signaling pathway of host cells within human breast cancer cell (BCC) xenografts in nude mice. *AACR Annual Meeting* 2013: Abstract# 1413.

Neve RM, Chin K, Fridlyand J, Yeh J, Baehner FL, Fevr T, Clark L, Bayani N, Coppe JP, Tong F, Speed T, Spellman PT, DeVries S, Lapuk A, Wang NJ, Kuo WL, Stilwell JL, Pinkel D, Albertson DG, Waldman FM, McCormick F, Dickson RB, Johnson MD, Lippman M, Ethier S, Gazdar A, Gray JW (2006) A collection of breast cancer cell lines for the study of functionally distinct cancer subtypes. *Cancer Cell* **10**(6): 515–527.

Nielsen TO, Hsu FD, Jensen K, Cheang M, Karaca G, Hu Z, Hernandez-Boussard T, Livasy C, Cowan D, Dressler L, Akslen LA, Ragaz J, Gown AM, Gilks CB, van de Rijn M, Perou CM (2004) Immunohistochemical and clinical characterization of the basal-like subtype of invasive breast carcinoma. *Clin Cancer Res* **10**(16): 5367–5374.

Okouneva T, Azarenko O, Wilson L, Littlefield BA, Jordan MA (2008) Inhibition of centromere dynamics by eribulin (E7389) during mitotic metaphase. *Mol Cancer Ther* **7**(7): 2003–2011.

Perou CM, Sorlie T, Eisen MB, van de Rijn M, Jeffrey SS, Rees CA, Pollack JR, Ross DT, Johnsen H, Akslen LA, Fluge O, Pergamenschikov A, Williams C, Zhu SX, Lonning PE, Borresen-Dale AL, Brown PO, Botstein D (2000) Molecular portraits of human breast tumours. *Nature* **406**(6797): 747–752.

Polyak K, Weinberg RA (2009) Transitions between epithelial and mesenchymal states: acquisition of malignant and stem cell traits. *Nat Rev Cancer* **9**(4): 265–273.

Sequist LV, Waltman BA, Dias-Santagata D, Digumarthy S, Turke AB, Fidias P, Bergethon K, Shaw AT, Gettinger S, Cosper AK, Akhavanfard S, Heist RS, Temel J, Christensen JG, Wain JC, Lynch TJ, Vernovsky K, Mark EJ, Lanuti M, Iafrate AJ, Mino-Kenudson M, Engelman JA (2011) Genotypic and histological evolution of lung cancers acquiring resistance to EGFR inhibitors. *Sci Transl Med* **3**(75): 75ra26.

Shah SP, Roth A, Goya R, Oloumi A, Ha G, Zhao Y, Turashvili G, Ding J, Tse K, Haffari G, Bashashati A, Prentice LM, Khattra J, Burleigh A, Yap D, Bernard V, McPherson A, Shumansky K, Crisan A, Giuliany R, Heravi-Moussavi A, Rosner J, Lai D, Birol I, Varhol R, Tam A, Dhalla N, Zeng T, Ma K, Chan SK, Griffith M, Moradian A, Cheng SW, Morin GB, Watson P, Gelmon K, Chia S, Chin SF, Curtis C, Rueda OM, Pharoah PD, Damaraju S, Mackey J, Hoon K, Harkins T, Tadigotla V, Sigaroudinia M, Gascard P, Tlsty T, Costello JF, Meyer IM, Eaves CJ, Wasserman WW, Jones S, Huntsman D, Hirst M, Caldas C, Marra MA, Aparicio S (2012) The clonal and mutational evolution spectrum of primary triple-negative breast cancers. *Nature* **486**(7403): 395–399.

Shankar DB, Li J, Tapang P, Owen McCall J, Pease LJ, Dai Y, Wei RQ, Albert DH, Bouska JJ, Osterling DJ, Guo J, Marcotte PA, Johnson EF, Soni N, Hartandi K, Michaelides MR, Davidsen SK, Priceman SJ, Chang JC, Rhodes K, Shah N, Moore TB, Sakamoto KM, Glaser KB (2007) ABT-869, a multitargeted receptor tyrosine kinase inhibitor: inhibition of FLT3 phosphorylation and signaling in acute myeloid leukemia. *Blood* **109**(8): 3400–3408.

Shipitsin M, Campbell LL, Argani P, Weremowicz S, Bloushtain-Qimron N, Yao J, Nikolskaya T, Serebryiskaya T, Beroukhim R, Hu M, Halushka MK, Sukumar S, Parker LM, Anderson KS, Harris LN, Garber JE, Richardson AL, Schnitt SJ, Nikolsky Y, Gelman RS, Polyak K (2007) Molecular definition of breast tumor heterogeneity. *Cancer Cell* **11**(3): 259–273.

Smith JA, Wilson L, Azarenko O, Zhu X, Lewis BM, Littlefield BA, Jordan MA (2010) Eribulin binds at microtubule ends to a single site on tubulin to suppress dynamic instability. *Biochemistry* **49**(6): 1331–1337.

Takano S, Kanai F, Jazag A, Ijichi H, Yao J, Ogawa H, Enomoto N, Omata M, Nakao A (2007) Smad4 is essential for down-regulation of E-cadherin induced by TGF-beta in pancreatic cancer cell line PANC-1. *J Biochem* **141**(3): 345–351.

Taube JH, Herschkowitz JI, Komurov K, Zhou AY, Gupta S, Yang J, Hartwell K, Onder TT, Gupta PB, Evans KW, Hollier BG, Ram PT, Lander ES, Rosen JM, Weinberg RA, Mani SA (2010) Core epithelial-to-mesenchymal transition interactome gene-expression signature is associated with claudin-low and metaplastic breast cancer subtypes. *Proc Natl Acad Sci USA* **107**(35): 15449–15454.

Towle MJ, Nomoto K, Asano M, Kishi Y, Yu MJ, Littlefield BA (2012) Broad spectrum preclinical antitumor activity of eribulin (Halaven(R)): optimal effectiveness under intermittent dosing conditions. *Anticancer Res* **32**(5): 1611–1619.

Towle MJ, Salvato KA, Budrow J, Wels BF, Kuznetsov G, Aalfs KK, Welsh S, Zheng W, Seletsky BM, Palme MH, Habgood GJ, Singer LA, Dipietro LV, Wang Y, Chen JJ, Quincy DA, Davis A, Yoshimatsu K, Kishi Y, Yu MJ, Littlefield BA (2001) *In vitro* and *in vivo* anticancer activities of synthetic macrocyclic ketone analogues of halichondrin B. *Cancer Res* **61**(3): 1013–1021.

Tsukada T, Fushida S, Harada S, Terai S, Yagi Y, Kinoshita J, Oyama K, Tajima H, Ninomiya I, Fujimura T, Ohta T (2013) Low-dose paclitaxel modulates tumour fibrosis in gastric cancer. *Int J Oncol* **42**(4): 1167–1174.

Uramoto H, Iwata T, Onitsuka T, Shimokawa H, Hanagiri T, Oyama T (2010) Epithelial-mesenchymal transition in EGFR-TKI acquired resistant lung adenocarcinoma. *Anticancer Res* **30**(7): 2513–2517.

Yang J, Weinberg RA (2008) Epithelial-mesenchymal transition: at the crossroads of development and tumor metastasis. *Dev Cell* **14**(6): 818–829.

Yu M, Bardia A, Wittner BS, Stott SL, Smas ME, Ting DT, Isakoff SJ, Ciciliano JC, Wells MN, Shah AM, Concannon KF, Donaldson MC, Sequist LV, Brachtel E, Sgroi D, Baselga J, Ramaswamy S, Toner M, Haber DA, Maheswaran S (2013) Circulating breast tumor cells exhibit dynamic changes in epithelial and mesenchymal composition. *Science* **339**(6119): 580–584.

Supplementary Information accompanies this paper on British Journal of Cancer website (http://www.nature.com/bjc)